1-10-2003

# Networks with fourfold connectivity in two dimensions

Frédéric Tessier
*University of Ottawa*

David H. Boal
*Simon Fraser University*

Dennis E. Discher
*University of Pennsylvania*, discher@seas.upenn.edu

# Networks with fourfold connectivity in two dimensions

Frédéric Tessier,[1] David H. Boal,[2] and Dennis E. Discher[3]

[1]*Department of Physics, University of Ottawa, Ottawa, Ontario, Canada K1N 6N5*
[2]*Department of Physics, Simon Fraser University, Burnaby, British Columbia, Canada V5A 1S6*
[3]*School of Engineering and Applied Science, University of Pennsylvania, Philadelphia, Pennsylvania 19104-6315*

The elastic properties of planar, $C_4$-symmetric networks under stress and at nonzero temperature are determined by simulation and mean field approximations. Attached at fourfold coordinated junction vertices, the networks are self-avoiding in that their elements (or bonds) may not intersect each other. Two different models are considered for the potential energy of the elements: either Hooke's law springs or flexible tethers (square well potential). For certain ranges of stress and temperature, the properties of the networks are captured by one of several models: at large tensions, the networks behave like a uniform system of square plaquettes, while at large compressions or high temperatures, they display many characteristics of an ideal gas. Under less severe conditions, mean field models with more general shapes (parallelograms) reproduce many essential features of both networks. Lastly, the spring network expands without limit at a two-dimensional tension equal to the force constant of the spring; however, it does not appear to collapse under compression, except at zero temperature.

## I. INTRODUCTION

Two-dimensional networks are found in many cell structures, including the membrane-associated cytoskeleton of mammalian erythrocytes, the bacterial cell wall, and the nuclear lamina. The erythrocyte cytoskeleton is an example of a network with at least partial $C_6$ symmetry, in that the network elements are frequently connected at sixfold coordinated junctions [1,2]. However, networks with lower coordination (i.e., fewer linking elements per vertex), and hence lower symmetry than $C_6$, are also observed in nature. For example, the nuclear lamina contains junctions that have fourfold coordination (X shaped) [3]. Further, the cortical lattice of the auditory outer hair cell [4] and the peptidoglycan network of the bacterial cell wall [5] have T-shaped junctions of threefold coordination and obviously low symmetry. The properties of networks with symmetries lower than $C_6$ are not well documented.

Networks with sixfold symmetry are characterized by two independent elastic moduli, as are isotropic materials, and their behavior under stress and at finite temperature has been investigated both analytically and by simulation. Thus far, attention has focused on networks whose elements are beads and tethers or identical springs [6–8]. In particular, spring networks with $C_6$ symmetry have been shown to expand without bound when the in-plane tensile stress exceeds a specific, temperature-independent threshold, and to collapse when the compressive stress exceeds a temperature-dependent threshold. The elastic moduli are stress dependent, with the area compression modulus vanishing at the expansion point, as one would expect.

In this paper, we explore the characteristics of networks with fourfold connectivity, a sample configuration at finite temperature being shown in Fig. 1. We refer to these systems as square or $C_4$-symmetric networks, reflecting the elementary plaquette shape or symmetry under tension. Of course, this is just the simplest example of a $C_4$-symmetric system: more complex connectivities also are permitted. In many cel-

lular examples of $C_4$ networks, out-of-plane fluctuations are suppressed because the network is held against a membrane having modest bending resistance. In this paper, we study networks confined to a plane, recognizing that transverse fluctuations will modify some of the predicted elastic behavior. We consider two different forms for the potential energy of a single network element. In one approach, the elements are ideal Hookean springs of force constant $k_{sp}$. This model mimics the behavior of a polymer network at modest deformations, but is not physical at two-dimensional tensions greater than $k_{sp}$, where the network expands without bound. To investigate these latter conditions, we employ a network of flexible tethers obeying a square well potential in which network elements have a fixed maximal extension. Not only is this network more physical at large deformations, it is also
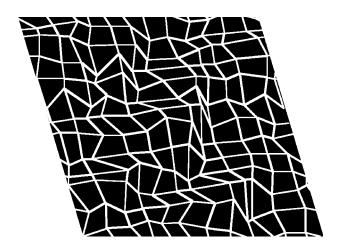


FIG. 1. Snapshot of a square network of Hookean springs with spring constant $k_{sp}$ and unstressed spring length $s_0$. This two-dimensional network patch is subject to nonorthogonal periodic boundary conditions, as indicated by the black background. Results are from a Monte Carlo simulation performed at a temperature $k_B T$ of $(1/4)k_{sp}s_0^2$ where $k_B$ is Boltzmann's constant. The configuration has been rotated so that one of its axes lies along the $x$ axis.

well described by a simple mean field representation. In both cases, the networks are self-avoiding in that their elements are not permitted to cross one another.

In Sec. II, we demonstrate how the deformation energy of square networks can be expressed in terms of three elastic moduli, one more than required for isotropic materials in two dimensions. Both the elastic moduli and the network geometry can be described by mean field approximations, several of which are presented in Secs. III and V for springs and tethers, respectively. In Sec. IV, a Monte Carlo simulation of a $C_4$ spring network is reported, including both the stress and temperature dependence of the network geometry and elastic properties; these results are compared with the mean field approaches. Tethered networks are treated in the same format: the mean field model in Sec. V and full simulations in Sec. VI. Our conclusions are summarized in Sec. VII. Lastly, the details of the simulation techniques are included in an Appendix.

## II. ELASTIC MODULI

When an object deforms in response to a stress, a given element of the object moves from its original position $\mathbf{x}$ to a new position $\mathbf{x}'$ by a displacement $\mathbf{u}$, where $\mathbf{u}$ varies locally across the object. The relevant description of the deformation is the strain tensor $u_{ij}$, which is related to the rate of change of $\mathbf{u}$ with position $\mathbf{x}$ through

$$u_{ij} = \frac{1}{2}\left[ \frac{\partial u_i}{\partial x_j} + \frac{\partial u_j}{\partial x_i} + \sum_k \frac{\partial u_k}{\partial x_i}\frac{\partial u_k}{\partial x_j} \right]. \quad (1)$$

In Hooke's law materials, the change in the free energy density $\Delta\mathcal{F}$ upon deformation is quadratic in the strain tensor $u_{ij}$:
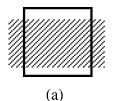
$$\Delta\mathcal{F} = \frac{1}{2}\sum_{ijkl} C_{ijkl}u_{ij}u_{kl} \quad (2)$$

where the material-specific constants $C_{ijkl}$ are the elastic moduli. In two dimensions, the symmetry of $u_{ij}$ under exchange of $i$ and $j$ reduces the number of independent moduli from $2^4$ to six. In addition, symmetry of the $C_4$ network under $x \rightarrow -x$ and $y \rightarrow -y$ shows that all components of $C_{ijkl}$ with an odd number of $x$ or $y$ indices must vanish, further reducing the number of independent moduli to four. Lastly, the fourfold rotational symmetry of the network ($x \rightarrow -y$ and $y \rightarrow x$) provides yet another relation among the moduli.

Hence, the free energy density involves just three independent elastic moduli, and can be written in the form

$$\Delta\mathcal{F} = (K_A/2)(u_{xx}+u_{yy})^2 + (\mu_p/2)(u_{xx}-u_{yy})^2 + 2\mu_s u_{xy}^2, \quad (3)$$

where the few independent combinations of $C_{ijkl}$ have been replaced by the area compression modulus $K_A$, the pure shear modulus $\mu_p$, and the simple shear modulus $\mu_s$. The deformation modes associated with pure and simple shear are illustrated in Fig. 2. Note that $\mu_p = \mu_s$ for isotropic ma-
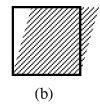


FIG. 2. Two potentially inequivalent shear modes in $C_4$ systems: (a) is pure shear and (b) is simple shear. The line outline shows the unstressed object, while the cross-hatched region shows the deformed object.

terials or triangular networks under infinitesimal deformation (see Ref. [9] for further reading).

## III. MEAN FIELD APPROXIMATIONS FOR SPRINGS

For many physical systems, the change in free energy density arising from a modest deformation varies quadratically in the magnitude of the deformation with respect to a reference configuration. The microscopic representation of such systems may include a network of elements with a deformation energy that is quadratic in their extension (i.e., springs) or in the angular separation between their nearest neighbors. The simplest of these networks involves identical Hookean springs (each with a force constant of $k_{\text{sp}}$ and an unstretched length of $s_0$) without explicit dependence upon the angles between neighboring elements. At low temperature or high tension, triangular networks of such springs have been successfully described by a mean field approach in which all triangular plaquettes of the network are equilateral [6–8].

In the simplest mean field approach, a network is tiled with identical plaquettes, such as triangles in $C_6$ networks or parallelograms in $C_4$. Why this approximation is so successful in $C_6$ spring networks is that the dominant plaquette shape at low temperature or high tension is an equilateral triangle, although the length of each side is not necessarily $s_0$. However, even fourfold networks of springs (let alone tethers) have a degenerate ground state at zero stress, as illustrated by the equal-energy configurations shown in Fig. 3(a). From simulations, the area per plaquette of this network is $0.6 s_0^2$, well below the $s_0^2$ of identical square plaquettes. Nevertheless, at least three mean field approximations are useful for describing $C_4$ networks of springs and all are
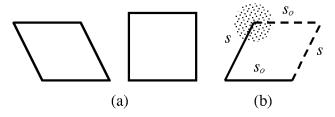


FIG. 3. (a) The ground state of the $C_4$ spring network is not unique at zero stress: each of these plaquettes has the same energy. (b) In the variable shape (VS) mean field model, a set of plaquette shapes is generated by sampling the position of the point indicated by the dotted region. The resulting parallelogram has two sides of length $s$ and two of $s_0$.

based on the enthalpy for a single plaquette with the shape of a parallelogram

$$H_{\text{plaquette}} = (k_{\text{sp}}/2)\{(s_1 - s_0)^2 + (s_2 - s_0)^2\} - \tau A, \quad (4)$$

where pairs of sides have lengths $s_1$ and $s_2$. The number of plaquettes in the network equals the number of vertices, but is half the number of springs.

In one approximation, all lengths and angles in the network are identical; we refer to this as the square plaquette or SP model. In a related approximation, the sides are fixed at $s_1 = s_2 = s_0$ and the acute included angle $\theta$ is allowed to change; we designate this as the variable angle or VA model. In the least restrictive approach, the plaquettes are identical parallelograms with one side of fixed length; we call this the variable shape or VS model. All three models are most useful at low temperature where the spring lengths are relatively constant: square plaquettes should dominate at high tension, while parallelograms (either VA or VS) are more appropriate near zero stress. Our objective here is to obtain a set of analytical solutions which can be used for such specific conditions. In terms of plaquette variables, we have chosen to remain close to the mean characteristics of the network (for instance, two degrees of translational freedom per plaquette), although we will mention alternative approaches. We have not evaluated the accuracy of a broad collection of mean field models, nor have we discovered one approximation that is valid under all conditions.

### A. Square plaquette and variable angle approximations

In the square plaquette approximation, all plaquettes are identical squares with a length $s_0$ to the side when unstressed, and $s_\tau$ to the side when subject to a two-dimensional tension $\tau$. The enthalpy per network vertex $H_{\text{SP}}$ of this model is

$$H_{\text{SP}} = k_{\text{sp}}(s - s_0)^2 - \tau s^2, \quad (5)$$

where each square plaquette has an area per vertex of $s^2$. At zero temperature, the spring length in this approximation is obtained by minimizing the enthalpy per vertex through the condition $\partial H_{\text{SP}}/\partial s = 0$. This yields a spring length at a tension $\tau$ of

$$s_\tau = s_0/(1 - \tau/k_{\text{sp}}) \quad \text{(SP model).} \quad (6)$$

From this expression, one can see that the spring length and area per vertex expand without bound beyond a tension given by

$$\tau_{\text{exp}} = k_{\text{sp}}. \quad (7)$$

By substituting Eq. (6) into Eq. (5), one arrives at

$$H_{\text{SP}} = k_{\text{sp}} s_0^2/(1 - k_{\text{sp}}/\tau) = k_{\text{sp}} s_0^2/(1 + k_{\text{sp}}/\Pi) \quad (8)$$

where $\Pi = -\tau$ is the pressure. For networks under compression, Eq. (8) establishes that $H_{\text{SP}} > 0$ for $\Pi > 0$.

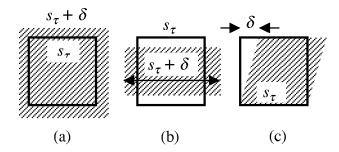Lifting the right-angle constraint but keeping the sides with fixed length $s_0$ leads to the expression



FIG. 4. Infinitesimal deformations of a square consisting of springs stretched from their unstressed length $s_0$ to a stretched length of $s_\tau$. The stretched square is shown in outline with a black border, and the infinitesimal deformation is shown as the cross-hatched region. Mode (a) measures the area compression modulus, while modes (b) and (c) measure the pure and simple shear moduli, respectively.

$$H_{\text{VA}} = \Pi s_0^2 \sin \theta, \quad 0 \leq \theta \leq \pi/2, \quad (9)$$

for the enthalpy in the VA model, where $\theta$ is the acute angle between neighboring sides of the plaquette. For $\Pi > 0$, $H_{\text{VA}}$ vanishes at $\theta = 0$, which corresponds to the shear collapsed state of lower ($C_2$) symmetry. Importantly, this configuration has a lower enthalpy than Eq. (8) for all $\Pi > 0$. Hence, $C_4$ networks at zero temperature are expected to collapse toward $C_2$ networks under any positive pressure:

$$\Pi_{\text{coll}} > 0 \quad \text{or} \quad \tau_{\text{coll}} < 0 \quad \text{(VA model).} \quad (10)$$

This behavior is similar to triangular networks of springs at zero temperature, which expand without bound when the in-plane tension exceeds $\sqrt{3} k_{\text{sp}}$, and collapse when the pressure (negative tension) is beyond $\sqrt{3} k_{\text{sp}}/8$.

For $\Pi < 0$ (tension), the VA model gives an area per plaquette of $A_v = s_0^2$ (with $\theta = \pi/2$) rather than $A_v = 0$ (with $\theta = 0$ for $\Pi > 0$). Yet even though the enthalpy is lower for the VA model under tension than for the SP model, the constant length constraint is unphysical at high positive tensions. Thus, the VA model primarily serves to prove that there is a symmetry-breaking step change at $\Pi = 0$ as $\theta$ switches from 0 to $\pi/2$ and the enthalpy changes from $H_{\text{VA}} = 0$ to $H_{\text{VA}} = -\tau s_0^2$. However, the SP model needs to be used to more accurately estimate the latter enthalpy.

Before proceeding to the third mean field model and full network simulations, we express the elastic moduli in terms of spring variables. This is done by determining the change in the free energy density at zero temperature for the deformation modes in Fig. 4 using two different expressions, namely, Eqs. (3) and (4), noting that Eq. (4) must be divided by $s_\tau^2$ to obtain an energy density. The changes in the free energy density, as well as the strain tensor, are given in Table I for modes (a)–(c) of Fig. 4. Comparing columns 2 and 4 of Table I yields the following expressions for the stress dependence of the elastic moduli in the SP approximation:

$$K_A = (k_{\text{sp}} - \tau)/2, \quad (11)$$

$$\mu_p = (k_{\text{sp}} + \tau)/2 \quad \text{(square plaquettes, } T = 0, \ \tau \neq 0\text{),} \quad (12)$$

TABLE I. Change in free energy density $\Delta\mathcal{F}$ for deformation modes (a), (b), and (c) in Fig. 4 of a square network of springs under stress. Column 2 (microscopic) refers to the enthalpy change expressed in spring variables, while column 4 (continuum) is the free energy change using Eq. (3) and the strain tensor in column 3.

| Mode | $\Delta\mathcal{F}$ (microscopic) | Strain | $\Delta\mathcal{F}$ (continuum) |
|------|------|------|------|
| (a) | $(k_{sp}-\tau)(\delta/s_\tau)^2$ | $u_{xx}=u_{yy}=\delta/s_\tau$ $u_{xy}=0$ | $2K_A(\delta/s_\tau)^2$ |
| (b) | $(k_{sp}+\tau)(\delta/s_\tau)^2$ | $u_{xx}=-\delta/s_\tau$ $u_{yy}=(1+\delta/s_\tau)^{-1}-1$ $u_{xy}=0$ | $2\mu_p(\delta/s_\tau)^2$ |
| (c) | $(\tau/2)(\delta/s_\tau)^2$ | $u_{xx}=u_{yy}=0$ $u_{xy}=(\delta/2s_\tau)$ | $(\mu_s/2)(\delta/s_\tau)^2$ |

$$\mu_s=\tau. \tag{13}$$

All three moduli are linear in the tension, and the simple shear modulus vanishes at zero tension, as expected. Further, the compression modulus decreases with increasing tension until it vanishes at the blow-up point for the area $\tau_{exp}=k_{sp}$; both shear moduli increase linearly with tension.

### B. Variable shape approximation

Parallelograms represent a less restrictive set of plaquette shapes. There are different algorithms for sampling the ensemble of parallelogram shapes, corresponding to different weights for each shape. The approach taken here is to fix one side to have a length $s_0$, with the shape being determined by a point moving randomly in a two-dimensional plane, as indicated by the shaded region in Fig. 3(b). A line drawn from the point to one end of the fixed side determines the length $s$ and angle $\theta$ of the second side of the parallelogram. The remaining two sides are determined by symmetry. An alternative approach, which permits two vertices of a parallelogram to move independently, involves four degrees of translational freedom per plaquette, rather than two degrees of freedom in either the VS model or the network as a whole. Introducing two extra degrees of freedom appears to compromise the accuracy of the VS approximation.

One of these extra degrees of freedom can be removed by forcing one side of the parallelogram to lie in a fixed direction, so that there are just three degrees of freedom per plaquette, one more than the network as a whole. For spring networks at low temperatures and zero stress, this model displays the same temperature dependence as the VS model to first order. Differences between the mean field models are more apparent at nonzero stress and temperature, but are not so great as to rule out one of the approximations. Please note that these conclusions apply only to $C_4$ networks; networks with higher connectivity, like $C_6$, behave differently because of the coupling between adjacent plaquette sides introduced by the extra bonds.

Our mean field model can be evaluated analytically at zero tension ($\tau=0$) and low temperature ($k_BT\ll k_{sp}s_0^2$); the model can be treated at arbitrary tension and temperature by numerical integration [10]. Each plaquette corresponds to two springs, one of length $s$ and the other $s_0$, such that the potential energy per plaquette is

$$E=(k_{sp}/2)(s-s_0)^2. \tag{14}$$

We introduce two dimensionless variables

$$\alpha=\beta k_{sp}s_0^2/2, \tag{15a}$$

$$\sigma=s/s_0, \tag{15b}$$

permitting the Boltzmann factor for a single vertex (or a single plaquette) to be written as

$$\exp(-\beta E)=\exp(-\beta k_{sp}[s-s_0]^2/2)=\exp(-\alpha[\sigma-1]^2). \tag{16}$$

In the above expressions, the inverse temperature is $\beta=(k_BT)^{-1}$, where $k_B$ is Boltzmann's constant.

Equation (16) can be used to construct a probability distribution for plaquette shapes. The mobile vertex which defines the plaquette shape moves in a two-dimensional plane. We define $\mathcal{P}(\sigma)\sigma\,d\sigma\,d\theta$ as the probability of finding the mobile vertex in the range $\sigma\,d\sigma\,d\theta$ around the location $(\sigma,\theta)$ in polar coordinates. As Eq. (16) does not depend upon $\theta$, the probability is

$$\mathcal{P}(\sigma)\sigma\,d\sigma=\frac{\exp(-\alpha[\sigma-1]^2)\sigma\,d\sigma}{\int\exp(-\alpha[\alpha-1]^2)\sigma\,d\sigma}. \tag{17}$$

The ensemble average of the area per vertex in the VS model (with one side of the plaquette of fixed length $s_0$) is

$$\langle A_v\rangle=s_0\langle s\rangle\langle\sin\theta\rangle=(2/\pi)s_0^2\langle\sigma\rangle, \tag{18}$$

where

$$\langle\sigma\rangle=\int_0^\infty\sigma\mathcal{P}(\sigma)\sigma\,d\sigma=\frac{\int\exp(-\alpha[\sigma-1]^2)\sigma^2d\sigma}{\int\exp(-\alpha[\sigma-1]^2)\sigma\,d\sigma}. \tag{19}$$

At low temperature, the integrands in Eq. (19) are concentrated around $\sigma=1$, and it is convenient to change variables to

$$\varepsilon=\sigma-1, \tag{20}$$

so that Eq. (19) becomes

$$\langle\sigma\rangle=\frac{\int_{-1}^\infty\exp(-\alpha\varepsilon^2)(\varepsilon+1)^2d\varepsilon}{\int_{-1}^\infty\exp(-\alpha\varepsilon^2)(\varepsilon+1)d\varepsilon}. \tag{21}$$

Expanding the polynomials in Eq. (21) leads to a number of integrals of the form

$$\int\exp(-\alpha\varepsilon^2)\varepsilon^n d\varepsilon=\alpha^{-(n+1)/2}\int\exp(-\xi^2)\xi^n d\xi, \tag{22}$$

where the integration limits on $\xi$ are from $-\sqrt{\alpha}$ to $+\infty$. Equation (15a) shows that $\alpha$ tends to infinity at low temperature; as a consequence, the integrands are approximately

symmetric about $\xi = 0$ at low temperature, and integrals with odd $n$ must vanish. Integrals even in $\xi$ are easy to evaluate, leading to

$$\langle \sigma \rangle = 1 + \frac{1}{2\alpha} \tag{23}$$

so that the area per vertex is

$$\langle A_v \rangle = \frac{2}{\pi} s_0^2 \left( 1 + \frac{k_B T}{k_{sp} s_0^2} \right). \tag{24}$$

From Eq. (24), the VS approximation predicts that the plaquette area will increase linearly with temperature, corresponding to a positive thermal expansion coefficient. This is in contrast to $C_6$ networks which display a negative thermal expansion coefficient both in simulations and in other theoretical approaches [11]. With one side of fixed length, pure dilations are not achievable in the VS model, so that the area compression modulus cannot be extracted directly from fluctuations in area. We return to this point in Sec. V.

## IV. SIMULATION OF SPRING NETWORKS

As emphasized in Sec. III, square networks assume a broad range of configurations at any given temperature and pressure, except when the network is placed under large tension and the elementary plaquettes are stretched into squares. Such a large configuration space is difficult to treat by analytic approximation, so we have recourse to computer simulations to determine the characteristics of spring networks at arbitrary temperature and pressure. The simulations involve standard Monte Carlo algorithms [6,7,12] for the isobaric isothermal ensemble, and are presented in more detail in the Appendix. In essence, the Monte Carlo procedure generates a set of configurations which correctly samples the integrand of the partition function, and from which statistically significant ensemble averages can be extracted.

We begin our presentation of the simulation results with the behavior of the network area and then move on to elastic moduli. Figure 5 shows the area per junction vertex $\langle A \rangle / N_j s_0^2$ (or the area per plaquette) as a function of tension, which is quoted as the dimensionless ratio $\tau / k_{sp}$ (negative values of $\tau$ correspond to pressure). The figure contains the square plaquette prediction found by squaring Eq. (6), as well as the simulation results for several temperatures: $k_B T / k_{sp} s_0^2 = 1/32, 1/16, 1/4,$ and 1. First, note that the general features of the SP model are reflected in the simulation of the full network. Indeed, the agreement is at the factor of 2 level for a significant fraction of the range of tensions shown in the figure, and the agreement is particularly good at large $\tau / k_{sp}$ where the network is stretched into square plaquettes.

Under compression, the values of $\langle A_v \rangle / s_0^2$ in the network are much lower than the SP prediction at low temperatures, i.e., $k_B T / k_{sp} s_0^2 \lesssim 1/16$. At the lowest temperature displayed ($k_B T / k_{sp} s_0^2 \lesssim 1/32$) the drop in the area below $\tau = 0$ is a hint of the collapse transition referred to in Eq. (10) for the variable angle model, although it may be that the temperature is
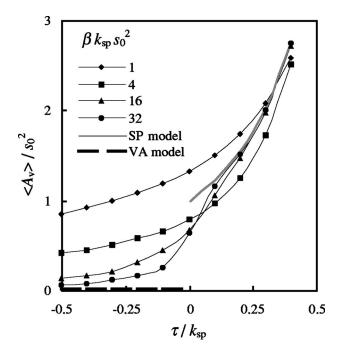


FIG. 5. Area per junction vertex $\langle A_v \rangle / s_0^2$ of a spring network as a function of reduced tension $\tau / k_{sp}$. The predictions of the square plaquette (SP) and variable angle (VA) approximations are compared with the full network simulation for several temperatures: $\beta k_{sp} s_0^2 = 32, 16, 4,$ and 1. Negative tension corresponds to pressure.

simply too high even at $k_B T / k_{sp} s_0^2 = 1/32$ for the transition to be visible in a $C_4$ network. In comparison, the collapse transition is clearly visible in triangular networks at this temperature. We conclude that square networks possess a collapse transition only at the lowest (if not zero) temperatures, with the much larger configuration space available to square networks removing the transition at modest temperatures.

At large compressions and high temperatures, we expect that the presence of the network springs is unimportant to some physical properties, and the vertices should behave more like an ideal gas. That is, at large compressions, $\langle A_v \rangle / s_0^2$ should approach the ideal gas limit of $1/\beta \Pi s_0^2$, where $\Pi = -\tau$ is the pressure. Certainly, the SP prediction of Eq. (6) does *not* possess this limit. The asymptotic behavior of the network area can be obtained by plotting the area as a function of $1/\beta \Pi s_0^2$, which is done in Fig. 6, where high pressures are on the left-hand side of the figure. The ideal gas behavior of the network is most apparent at $1/\beta \Pi s_0^2 < 0.2$; the lowest temperature system ($k_B T / k_{sp} s_0^2 = 1/32$) is the first to deviate from an ideal gas.

The area compression modulus is presented in Fig. 7, where the reduced modulus $K_A / k_{sp}$ is plotted against the reduced tension $\tau / k_{sp}$, a choice of variables suggested by the mean field expression Eq. (11). For stretched networks at low temperature ($k_B T / k_{sp} s_0^2 < 1/4$), the compression modulus tracks the square plaquette prediction remarkably well over a broad range of tension, and vanishes at $\tau = k_{sp}$ as predicted by Eq. (11). Of course, this is not a surprise given the good agreement of the SP prediction displayed in Fig. 5 for the same range of conditions. However, for modest tensions, or
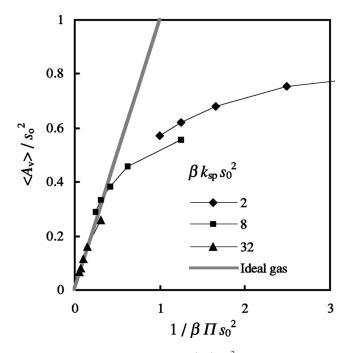
FIG. 6. Area per junction vertex $\langle A_v \rangle / s_0^2$ for a spring network under compression $\Pi = -\tau$. The area is plotted as a function of $1/\beta \Pi s_0^2$ (high pressure on the left-hand side of the graph) so that the ideal gas prediction for the area is just a straight line with unit slope. The full network simulation is shown for $\beta k_{sp} s_0^2 = 2$, 8, and 32.



FIG. 7. Area compression modulus $K_A / k_{sp}$ of a spring network shown as a function of reduced tension $\tau / k_{sp}$. The full network simulation is shown for $\beta k_{sp} s_0^2 = 32$, 16, 4, and 1. The square plaquette (SP) calculation is from Eq. (11). The ideal gas expectation for the compression modulus is $K_A = \Pi = -\tau$.

networks under compression, the agreement is nowhere near as good, and the compression modulus drops below the square plaquette prediction for the two lowest temperatures, and lies above the SP prediction for the two highest temperatures. Also visible on Fig. 7, the compression modulus follows along the ideal gas value at low temperature and high pressure, where $K_A = \Pi = -\pi$. In addition, Fig. 7 illustrates that $K_A$ increases with temperature for networks under modest compression: $K_A$ is a factor of 3 higher at $k_B T / k_{sp} s_0^2 = 1$ than at $k_B T / k_{sp} s_0^2 = 1/16$ for tensions near zero. Lastly, $K_A$ drops near $\tau = 0$ for $k_B T / k_{sp} s_0^2 = 1/32$, reflecting the contraction in the network area seen in Fig. 5, although the behavior of $K_A$ does not appear to signal a phase transition.

The pure shear modulus is displayed as a function of temperature in Fig. 8. As expected, the agreement between the square plaquette approach and the full network is best when the network is stretched at $\tau / k_{sp} > 0.5$. Further, the general rise of $\mu_p / k_{sp}$ with increasing tension is also in moderately good agreement with the SP approximation. However, the behavior of the network under compression, or near zero pressure, is significantly different from the square mean field result. We do not believe that the nonzero value of $\mu_p$ at $k_B T / k_{sp} s_0^2 = 1/16$ and under compression is a finite size effect: no systematic decrease in $\mu_p$ is observed as the system size increases from 144 to 1600 vertices. Lastly, we present the simple shear modulus in Fig. 9. The network agrees with the square plaquette approximation of $\mu_s = \tau$ at the largest tensions for all temperatures considered. Further, the agreement with the SP model improves as the temperature decreases, and is excellent at $k_B T / k_{sp} s_0^2 = 1/32$.
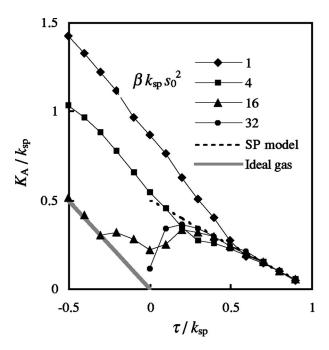
Although the area and the compression modulus display ideal gas behavior over a large range of compression, neither $\mu_p$ nor $\mu_s$ vanishes at high temperatures, contrary to ideal gas expectations. That the shear moduli are nonzero reflects how the presence of bonds tends to make the network more rigid, an effect noted in studies of other networks [13]. Fig-
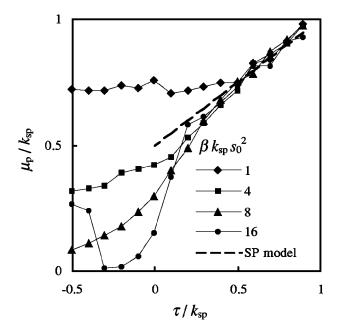


FIG. 8. Pure shear modulus $\mu_p / k_{sp}$ of a spring network shown as a function of reduced tension $\tau / k_{sp}$. The full network simulation is shown for $\beta k_{sp} s_0^2 = 16$, 8, 4, and 1. The square plaquette calculation is from Eq. (12).
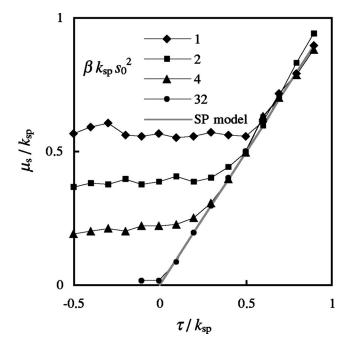
FIG. 9. Simple shear modulus $\mu_s/k_{sp}$ of a spring network shown as a function of reduced tension $\tau/k_{sp}$. The full network simulation is shown for $\beta k_{sp}s_0^2 = 32$, 4, 2, and 1. The square plaquette calculation is from Eq. (13).

ures 8 and 9 suggest that both $\mu_p$ and $\mu_s$ vanish under compression at zero temperature.

Figures 5–9 emphasize the stress dependence of the network by plotting results at fixed temperature. In Figs. 10 and 11 we show a selection of simulation results plotted as a
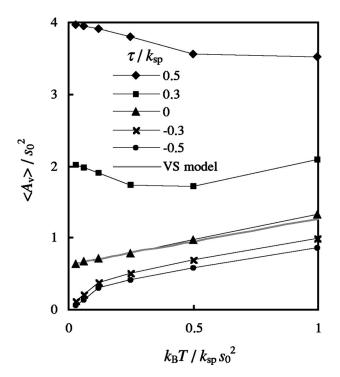


FIG. 10. Temperature dependence of the area per junction vertex $\langle A_v\rangle/s_0^2$ of a spring network for a selection of pressures with $k_B T/k_{sp}s_0^2 \leq 1$. The variable shape calculation is from Eq. (24).
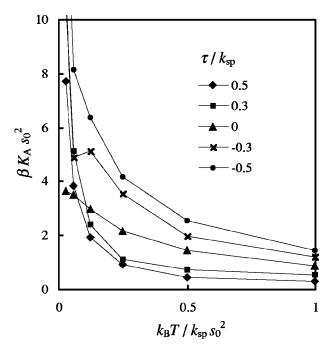


FIG. 11. Temperature dependence of the compression modulus $\beta K_A s_0^2$ for a spring network over a range of pressures with $k_B T/k_{sp}s_0^2 \leq 1$.

function of temperature at fixed stress. As shown in Fig. 10, the area per vertex both increases and decreases as a function of temperature, depending on the stress. The area increases with $T$ for all the systems under compression, implying that the network has a positive thermal expansion coefficient for $\Pi = -\tau > 0$. However, for some of the networks under tension, the area initially decreases with increasing temperature, corresponding to a negative thermal expansion coefficient (negative thermal expansion coefficients are also observed in $C_6$ networks [11]). Inspection of sample configurations demonstrates why this happens: at low temperatures and moderate tension, network plaquettes have the form of squares, with the spring lengths not too far from their unstressed values. As the temperature increases slowly from $T=0$, the spring lengths are still close to $s_0$, but the plaquettes become parallelograms and other shapes favored by entropy, resulting in a decrease of area. Figure 10 also displays the VS prediction of the network area at zero stress according to Eq. (24). Over the range of temperature investigated, the predicted values are in very good agreement with simulations. Lastly, the temperature dependence of the area compression modulus is displayed in Fig. 11. Not unexpectedly, the network softens as the temperature increases.

## V. MEAN FIELD MODEL FOR TETHERED NETWORKS

As with the spring network, we now ask whether there is a mean field model in which a single fluctuating plaquette roughly mimics the behavior of the network as a whole. As with the springs, our approach is to tile the network with parallelograms with one pair of sides having fixed length while the length of the other pair is determined by the position of a randomly moving vertex, as in Fig. 3(b). The fixed

side is chosen to have a length equal to the mean length of a tether in one dimension, namely, $s_{max}/2$. This is similar to choosing a length of $s_0$ for springs, although the low temperature fluctuations in tether length are dramatic compared to those of springs. Again, we note that this is just one algorithm for sampling the shapes of parallelograms; an inequivalent approach is to fix one vertex and allow two moving vertices to define two adjacent sides of the plaquette. However, introducing additional degrees of translational freedom reduces the accuracy of the model.

We evaluate this model analytically at zero tension (for $\tau \neq 0$, the calculation can be performed numerically, as demonstrated in Ref. [10]). With one side fixed, the mean area per plaquette is simply

$$\frac{\langle A \rangle}{N} = \frac{\frac{1}{2} \int_0^\pi \int_0^{s_{max}} s_{max} s^2 \sin\theta \, d\theta \, ds}{\int_0^\pi \int_0^{s_{max}} s \sin\theta \, d\theta \, ds} = \frac{2 s_{max}^2}{3\pi}. \quad (25)$$

The elastic moduli can be obtained from the fluctuations in the height of a parallelogram with a fixed base. When $u_{xx}$ vanishes on account of the fixed length of the parallelogram base, Eq. (A3) for the free energy density reads

$$\Delta \mathcal{F} = (K_A + \mu_p)(u_{yy}^2/2) + 2\mu_s u_{xy}^2. \quad (26)$$

The same logic that leads to Eqs. (A4)–(A6) now gives

$$\beta(K_A + \mu_p)\langle A_v \rangle = \frac{1}{\langle u_{yy}^2 \rangle} = \frac{\langle y \rangle^2}{\langle y^2 \rangle - \langle y \rangle^2}, \quad (27)$$

$$\beta\mu_s \langle A_v \rangle = \frac{1}{4\langle u_{xy}^2 \rangle} = \frac{\langle y \rangle^2}{\langle x^2 \rangle - \langle x \rangle^2}, \quad (28)$$

where $(x,y)$ are the coordinates of the moving vertex and $\langle A_v \rangle$ is the mean area of the parallelogram, from Eq. (25) with one vertex per plaquette. It is trivial to show that $\langle x^2 \rangle = \langle y^2 \rangle = s_{max}^2/4$ and $\langle y \rangle = 4 s_{max}/3\pi$, so that

$$\beta(K_A + \mu_p)s_{max}^2 = 4\pi \cong 12.6, \quad (29)$$

$$\beta\mu_s s_{max}^2 = 32/3\pi \cong 3.40 \quad \text{(mean field for tethers)}. \quad (30)$$

The elastic moduli under tension can be obtained by numerical integration [10].

## VI. SIMULATIONS OF TETHERED NETWORKS

The first thing to note about tethers compared to springs is that, while the square well potential sets a fundamental length scale $s_{max}$ for the network, it does not provide an energy scale. Thus, the only independent thermodynamic parameter in the network is the dimensionless combination $\tau s_{max}^2/k_B T$, where $\tau$ is the two-dimensional tension, as usual. The mean area per vertex $\langle A_v \rangle = \langle A \rangle/N$ is displayed as a function of this parameter in Fig. 12. Under compression, the area approaches that of an ideal gas $\langle A_v \rangle = k_B T/\Pi$, where the pressure $\Pi$ is equal to $-\tau$, particularly for $\tau s_{max}^2/k_B T$
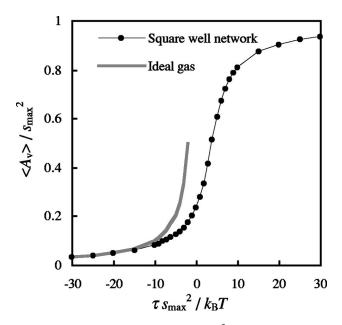


FIG. 12. Mean area per vertex $\langle A_v \rangle/s_{max}^2$ for a tethered network as a function of reduced tension $\tau s_{max}^2/k_B T$. Under moderate compression ($\tau s_{max}^2/k_B T < -10$), the system behaves like an ideal gas. Over the range of tensions displayed, the mean field predictions of Sec. V lie within a few percent of the data (see Ref. [10]).

$< -10$. Under tension ($\tau > 0$), the network initially expands rapidly, but finally approaches its asymptotic value of $\langle A_v \rangle/s_{max}^2 = 1$ dictated by the maximum tether length. This behavior is in contrast to springs, which can expand without limit. At zero stress, the numerical value of $\langle A_v \rangle/s_{max}^2$ is found to be 0.23, which is very close to $2/3\pi = 0.21$ predicted by the mean field approach of Eq. (25). In fact, when the parallelogram approximation of Sec. V is extended to nonzero tension [10], the predictions are within a few percent of the numerical results of Fig. 12.

The area compression modulus $K_A$ is proportional to the reciprocal of the tangent to the area vs tension curve, so we expect $K_A$ to diverge at large tension, where the area changes only very slowly. This behavior can be seen in Fig. 13, where $K_A$ clearly increases with tension. Thus, the vanishing of $K_A$ under tension seen in spring networks in Fig. 7 is absent with tethers. However, the behavior of the shear moduli is similar in the two networks: the plaquettes in both networks fluctuate ever more tightly about square shapes at large tension, meaning that their shear resistance increases. This feature can be seen in Fig. 13 for tethers, and in Figs. 8 and 9 for springs. Indeed, a linear increase in shear resistance with tension can be observed in all of these figures. At zero stress, the sum $\beta(K_A + \mu_p)s_{max}^2$ from Fig. 13 is 11.7, close to the mean field prediction of Eq. (29). Similarly, the observed value of $\beta\mu_s s_{max}^2$ is 3.0, close to Eq. (30).

## VII. SUMMARY

We investigate two different planar networks with fourfold connectivity: $N$ vertices linked together by $2N$ structural elements, which may be either springs or tethers but are not allowed to cross one another. Examined at both nonvan-
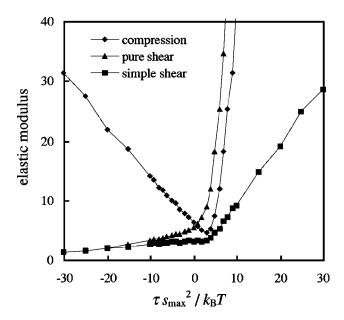
FIG. 13. Elastic moduli of tethered network as a function of the reduced tension $\tau s_{max}^2/k_B T$.

ishing temperature $T$ and tension $\tau$, the networks are described by three elastic moduli in two dimensions—the compression modulus $K_A$, pure shear modulus $\mu_p$, and simple shear modulus $\mu_s$. In general, the large fluctuations in network shape present even at $T=0$ require that the geometrical and elastic properties be determined by Monte Carlo simulation. However, under some conditions, the network can be described by one of several mean field approximations in which all plaquettes have the shape of squares or parallelograms.

Spring networks are useful for describing polymer systems at modest temperatures and stress. Our model system consists of identical springs with force constant $k_{sp}$ and unstressed length $s_0$. The simulations show that the area increases with tension until it expands without bound at $\tau = k_{sp}$. Correspondingly, the area compression modulus decreases with increasing tension until it vanishes at $\tau = k_{sp}$. The two shear moduli $\mu_p$ and $\mu_s$ increase with tension, as expected where the plaquettes become similar in shape (more resistance to shear) but fluctuate dramatically in size (less resistance to compression). When the network is subject to compression, its area and compression modulus (but not its shear moduli) approach those of an ideal gas. However, there does not appear to be a phase transition to a collapsed state except at zero temperature. This behavior is in contrast to triangulated networks, in which the collapse transition is clearly visible at a temperature-dependent threshold in stress.

Hookean springs do not provide an accurate description of a physical network at large stress because the spring can be stretched without limit. To provide insight into networks under these conditions, we also investigate tethered networks, in which the bond elements are hard tethers whose length may range freely between 0 and $s_{max}$ but not beyond. Tethered networks approach a maximal area of $Ns_{max}^2$ at large tension; their compression modulus necessarily diverges under these conditions, in contrast to ideal spring networks

where the compression modulus vanishes. Of course, the shear moduli also increase with tension just as they do for springs: at large tensions, the network plaquettes ever more resemble squares and resist deformation in their shape.

## ACKNOWLEDGMENTS

## APPENDIX: SIMULATION TECHNIQUE

The $C_4$ network in our simulations consists of $N$ vertices with fourfold connectivity, linked together by a total of $2N$ elements or bonds. The periodic network shape is described by two nonorthogonal vectors **U** and **V** which define the boundaries of the repeat unit, a parallelogram. For the spring network, the enthalpy $H$ is simply

$$H=(k_{sp}/2)\sum_i (s_i-s_0)^2 - \tau A \quad \text{(springs)}, \quad \text{(A1)}$$

where the sum is over all springs $i$ of the network, each with force constant $k_{sp}$ and unstressed length $s_0$. For a tethered network, the enthalpy just contains the term $-\tau A$, with the constraint that all bond lengths $s_i$ must be less than $s_{max}$. A configuration is propagated using a Monte Carlo technique in which trial moves are made on the positions of all vertices and on the boundary vectors of the network.

(i) Trial moves are made sequentially on the set of vertices by displacing each one randomly within a maximum distance $\Delta_v$ in each Cartesian direction, and evaluating the resulting change in enthalpy $\Delta H$ of a single vertex move. Clearly, a change in a vertex position may only result in a change in energy, since a vertex move does not change the area of the system. The move is accepted according to the conventional Boltzmann weight $\exp(-\beta\Delta H)$, where $\beta$ is the inverse temperature ($\beta^{-1}=k_B T$).

(ii) Trial moves are made on the two boundary vectors **U** and **V** by displacing each one randomly within a maximum distance $\Delta_b$ in each Cartesian direction, and rescaling the positions of the vertices simultaneously. Changing the periodic container shape results in a change in area $\Delta A$ and a change in enthalpy $\Delta H$ from which a pseudo-Boltzmann weight

$$W=\exp[-\beta\Delta H + N\ln(1+\Delta A/A)] \quad \text{(A2)}$$

can be constructed [12]. One boundary rescaling is attempted for every $N$ positional moves (i.e., the procedure involves one trial move on each vertex, followed by one boundary rescaling).

The values of $\Delta_v$ and $\Delta_b$, while fixed during the simulation of a given $T$ and $\tau$, are adjusted to give reasonable acceptance rates.

In our calculational method, the elastic moduli are extracted from fluctuations in the shape of the periodic bound-

aries of the network. From Sec. II, the change in free energy density for deformations around an equilibrium state can be expressed in terms of the strain tensor $u_{ij}$ as

$$\Delta\mathcal{F}=(K_A/2)(u_{xx}+u_{yy})^2+(\mu_p/2)(u_{xx}-u_{yy})^2+2\mu_s u_{xy}{}^2.$$

$$\text{(A3)}$$

Being quadratic in the strain tensor combinations $u_{xx}+u_{yy}$, $u_{xx}-u_{yy}$, and $u_{xy}$, this expression implies that the fluctuations in these combinations should be Gaussian, with expectations

$$\langle(u_{xx}+u_{yy})^2\rangle=1/\beta K_A\langle A\rangle, \qquad \text{(A4)}$$

$$\langle(u_{xx}-u_{yy})^2\rangle=1/\beta\mu_p\langle A\rangle, \qquad \text{(A5)}$$

$$\langle u_{xy}{}^2\rangle=1/4\beta\mu_s\langle A\rangle. \qquad \text{(A6)}$$

The strain tensor can be written in terms of the boundary vectors **U** and **V** which have coordinates

$$\mathbf{U}=(L_x+\Delta_x,0) \quad \text{and} \quad \mathbf{V}=(\Delta_{yx},L_y+\Delta_y), \qquad \text{(A7)}$$

where $L_x$ and $L_y$ are the equilibrium values of the boundary vectors at a given temperature and pressure. Note that **U** has

been rotated so as to lie along the $x$ axis in this representation, even though **U** and **V** randomly sample Cartesian space in the simulation. In terms of the boundary vectors, Eq. (A4) corresponds to the familiar

$$1/\beta K_A=\langle\Delta A^2\rangle/\langle A\rangle. \qquad \text{(A8)}$$

Equations (A4) and (A5) can be combined to give

$$1/\beta\mu_p=(1/\beta K_A)-4\langle\Delta_x\Delta_y\rangle. \qquad \text{(A9)}$$

Finally, Eq. (A6) is just

$$1/\beta\mu_s=\langle A\rangle\langle(\Delta_{yx}/L_y)^2\rangle. \qquad \text{(A10)}$$

All of the simulations are performed with $N=196$, and a total of 2100 configurations are generated at each pressure/temperature combination, although the first 100 configurations are discarded to remove any dependence on the initial configuration. Each configuration in the ensemble is separated by 2000 attempted moves per vertex, which is a sufficiently large number to strongly reduce the correlation between successive configurations. With this data set, we estimate that the uncertainties in geometrical quantities such as the area are about 1%, and the uncertainties in the elastic moduli are about 10%.

[1] T. J. Byers and D. Branton, Proc. Natl. Acad. Sci. U.S.A. **82**, 6153 (1985).

[2] For a review, see T. L. Steck, in *Cell Shape: Determinants, Regulation and Regulatory Role*, edited by W. Stein and F. Bronner (Academic, New York, 1989), Chap. 8.

[3] U. Aebi, J. Cohn, L. Buhle, and L. Gerace, Nature (London) **323**, 560 (1986).

[4] M. C. Holley and J. F. Ashmore, Nature (London) **335**, 635 (1988); J. Cell. Sci. **96**, 283 (1990); M. C. Holley, F. Kalinec, and B. Kachar, *ibid.* **102**, 569 (1992).

[5] A. L. Koch, Am. Sci. **72**, 327 (1990).

[6] D. H. Boal, U. Seifert, and J. C. Shillcock, Phys. Rev. E **48**, 4274 (1993).

[7] D. E. Discher, D. H. Boal, and S. K. Boey, Phys. Rev. E **55**, 4762 (1997).

[8] W. Wintz, R. Everaers, and U. Seifert, J. Phys. I **7**, 1097 (1997).

[9] L. D. Landau and E. M. Lifshitz, *Theory of Elasticity* (Pergamon, London, 1959).

[10] F. Tessier, Ph.D. thesis, Simon Fraser University, 1999, p. 59.

[11] D. E. Discher and P. Lammert, Phys. Rev. E **57**, 4368 (1998).

[12] W. W. Wood, J. Chem. Phys. **48**, 415 (1968); see also J. P. Hansen and I. R. McDonald, *Theory of Simple Liquids* (Oxford University Press, New York, 1986).

[13] M. Plischke, D. C. Vernon, B. Joos, and Z. Zhou, Phys. Rev. E **60**, 3129 (1999).